Mol. Cryst. Liq. Cryst., 1981, Vol. 70, pp. 145–161
0026-8941/81/7001-0145 $06.50/0

Variable Grating Mode Liquid Crystal Device for Optical Processing and Computing†

B. H. SOFFER, J. D. MARGERUM, A. M. LACKNER and D. BOSWELL
Hughes Research Laboratories, 3011 Malibu Canyon Road, Malibu, California 90265

and

A. R. TANGUAY, JR., T. C. STRAND, A. A. SAWCHUK and P. CHAVEL‡
Image Processing Institute, University of Southern California, Los Angeles, California 90007

(Received August 12, 1980; in final form November 13, 1980)

Certain nematic liquid crystal mixtures are observed to form a "variable grating mode" (VGM) for appropriate choices of cell design and applied voltage. In this mode of operation, a phase grating in the plane of the cell arises from a periodic variation in the orientation of the liquid crystal director. The grating spatial frequency is observed to vary linearly as a function of the applied voltage above the formation threshold. Liquid crystal and device parameters characteristic of the observed variable grating mode are presented. Utilization of the VGM effect in a photoconductively-addressed device is shown to provide an intensity-to-spatial frequency conversion. Applications of this unique type of optical transducer to arbitrary nonlinear optical processing problems are described. Results of level slicing experiments and implementation of optical logic functions are presented.

I INTRODUCTION

The variable grating mode (VGM) effect, in which some nematic liquid crystal layers exhibit a laterally periodic optical phase characterized by a voltage dependent spatial frequency, has been observed by several authors.[1–6] A VGM liquid crystal device can be constructed with the addition of a photoconductive layer in series with the liquid crystal layer.[4] When utilized as an optical-to-

†Presented at the Eighth International Liquid Crystal Conference, Kyoto, 1980.
‡Permanent address: Institut d'Optique, Universite de Paris sud, Orsay, France.

optical image transducer, this device has the rather unique property of converting in real time the intensity of an input image into a spatial frequency. Such an intensity-to-spatial frequency converter can be employed to implement arbitrary nonlinear point operations on input images.

In section II of this paper, we describe our investigations on the VGM effect as a function of compositional differences in phenyl benzoate liquid crystal mixtures, from which we chose an ester mixture for use in our photoactivated device. The construction and operation of this VGM liquid crystal device is described in section III. The unique approach to real time point nonlinear optical processing offered by this device is illustrated in section IV. The principal advantages with respect to earlier point nonlinear optical processing schemes[7–12] including real time approaches[13–16] are discussed, especially for the implementation of optical binary logic operations.[17–19]

II VGM EFFECTS AND MATERIALS CONSIDERATIONS

In the variable grating mode operation of liquid crystals, a phase grating is formed with a period that depends upon the voltage placed across the cell. This phase grating originates from a variation of the optical path length due to a periodic orientational perturbation of the liquid crystal uniaxial index ellipsoid. The direction of periodicity is perpendicular to the quiescent state alignment of the liquid crystal molecules, i.e., the domains are parallel to the liquid crystal alignment in the off state. Typical spatial frequency variation is from 100 to 600 cycles/mm. Figure 1 shows typical voltage-induced behavior of a VGM cell as seen through a polarizing microscope. The period of the phase grating can be seen to decrease as the applied voltage increases. Some imperfections in the VGM device can also be observed in the photographs.

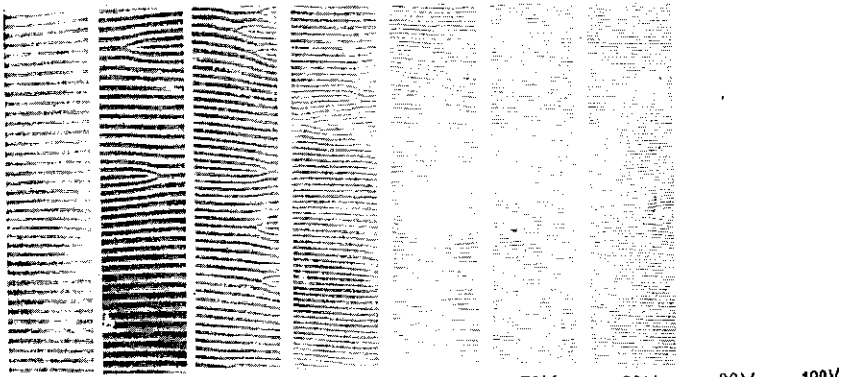

FIGURE 1 VGM viewed through polarizing microscope.

Inconsistencies in the grating alignment within each picture and from picture to picture may be noted. The optical diffraction patterns resulting from the phase grating in a typical VGM cell are shown in Figure 2.

We have observed VGM domains in planar cells up to about 13 μm in thickness of the liquid crystal. These VGM domains for static fields are always parallel to the quiescent state alignment direction on the electrode surface and are observed only with applied dc fields. These effects are entirely consistent with the experimental results of Barnik *et al.*,[6] but do not support other observations that the cells must be about 6 μm thick or less,[2,4,5] that the domain can be either parallel or perpendicular to the alignment direction,[2-5] and that ac activation can be used.[2] Our undoped liquid crystals were relatively high in resistivity ($> 10^{10}$ ohm-cm) and showed little or no dynamic scattering even at dc voltages as high as five times the threshold voltage.

The VGM effect in nematic-phase liquid crystals of negative dielectric anisotropy has been previously studied primarily with azoxy mixtures, such as Merck NP-V. These yellow-colored eutectic mixtures absorb light strongly in the near ultraviolet and blue (below 430 nm) region of the spectrum, and can undergo photodecomposition during extended illumination. We studied phenyl benzoate liquid crystal mixtures because they are colorless (strong absorption below 350 nm), are more stable to visible light exposures, and are more easily purified than the azoxy mixtures. Since we have been studying structural effects (particularly molecular length) on the anisotropic and dynamic scattering properties of a series of phenyl benzoate mixtures,[21] we ex-

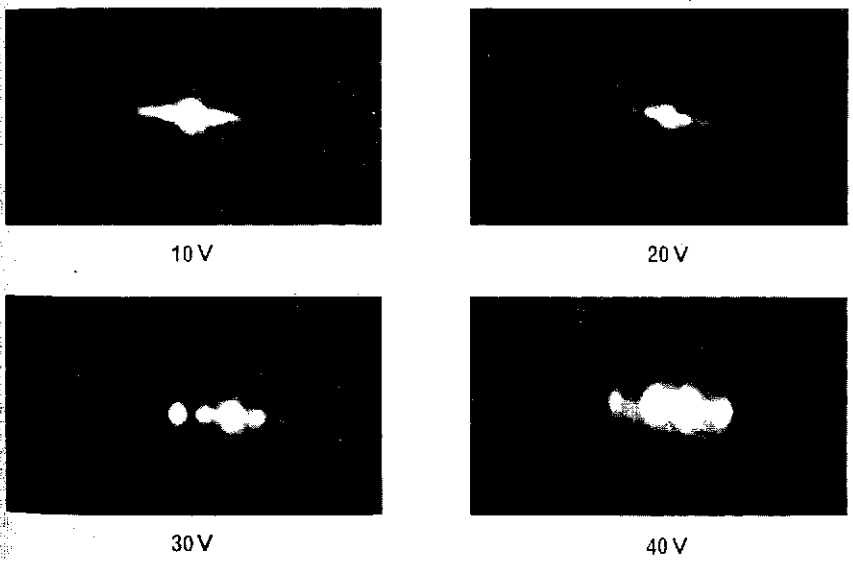

FIGURE 2 Diffraction patterns of a VGM cell.

amined the VGM response of this series as well as several other mixtures. The purpose was two-fold: (1) to select phenyl benzoate mixtures suitable for VGM studies in photoactivated devices, and (2) to look for correlations of structures or physical properties with the VGM effect. The materials studied are shown in Table I. Their VGM characteristics are compared with some of their anisotropic properties in Table II. The voltage dependence of their VGM domain grating frequency is shown in Figure 3.

Typical cells used in the foregoing experiments were fabricated from indium tin oxide (ITO)-coated, 1.27 cm or 0.32 cm thick optical flats. The liquid crystal layer was confined by a 6 μm Mylar perimeter spacer. The liquid crystal surface alignment was obtained by spin-coating an aqueous solution containing polyvinyl alcohol on the ITO-coated surfaces, drying at 100° C, and gently rubbing to give a uniform directionality. The effect of dc voltage was observed with a polarizing microscope at 258× magnification for each liquid crystal mixture. The width d of the domain period (line pair) is inversely proportional to applied voltage according to

$$d = \alpha / V \tag{1}$$

where α is a constant that is dependent on the particular liquid crystal mixture. This relationship is illustrated in Figure 3, in which dc voltage as a function of grating frequency $1/d$ for each eutectic mixture is a straight line with

TABLE I

Liquid crystal mixtures used for VGM studies

Class and Number	End Group Composition —Mole Fraction— Alkoxy/Alkyl	Dialkoxy	Dialkyl	Nematic Range mp, °C	clpt, °C	Average Length, Å
Azoxy						
Merck NP-V	1.000	—	—	−5	73	18.69
RO-R′ Esters[a]						
HRL-2N42	1.000	—	—	5	58	20.39
HRL-2N43	1.000	—	—	−6	52	22.37
HRL-2N42/48	1.000	—	—	2	57	23.36
HRL-2N44	1.000	—	—	−8	51	24.31
HRL-2N46	1.000	—	—	16	55	25.92
HRL-2N48	1.000	—	—	18	56	27.14
RO-OR′ Components[b]						
HRL-2N11	—	.428	.572	13	47	22.26
HRL-2N40	.755	.245	—	0	58	22.68
HRL-2N25	.772	.228	—	0	56	24.48

[a] RO-R′ refers to 4-alkoxyphenyl 4-alkylbenzoate esters. See Ref. 21 for the exact composition of these multicomponent mixtures.

[b] RO-OR′ refers to 4-alkoxyphenyl 4-alkoxybenzoate esters. See Refs. 22, 23, and 24 for the exact composition of 2N11, 2N40, and 2N25, respectively. The 2N11 mixture has a R-R′ component, 4 butylphenyl 4-toluate, and no RO-R′ components.

TABLE II

Liquid crystal anisotropic properties and VGM response

LC Number	Viscosity at 25°C (cP)	Δn at 22°C & 589 nm	AC-Resistivity $\rho_{\perp} \times 10^{11}$ (ohm-cm)	$\Delta\epsilon$ at 25°C & 5 KHz	V_{th} (volts)	VGM Characteristics[a] Width, d_{th} (μm)	Slope, α (Vmm/lp)
NP-V	24.9	0.290	2.0	−0.2	10	8.5	0.082
2N42	32.6	0.162	6.1	−0.22	10	5.4	0.099
2N43	36.5	0.148	7.2	−0.25	25	8.1	0.287
2N42/48	36.9	0.140	33.0	−0.29	35	5.6	0.340
2N44	38.1	0.136	10.0	−.030	—[b]	—	—
2N46	39.8	0.135	21.0	−0.30	—[b]	—	—
2N48	44.5	0.134	23.1	−0.33	—[b]	—	—
2N11	43.8	0.133	2.8	−0.5	15	5.1	0.122
2N40	46.9	0.151	8.5	0.28	16	4.3	0.089
2N25	48.5	0.139	11.0	−0.38	21	7.1	0.203

[a] The threshold voltage, V_{th}, is the lowest voltage at which the width of the domain period, d_{th}, was easily measured in cells with 6 μm spacers.
[b] No VGM observed up to 100 V dc.

slope α. Values of α for various liquid crystal mixtures are given in Table II. A smaller value of α is preferred, since a smaller slope gives a larger range of spatial frequency for the VGM effect per unit applied voltage. Thus, HRL-2N40 was chosen as the best of these ester liquid crystal mixtures for use in our studies of the photoactivated VGM device. The HRL-2N42 mixture is also of interest because its α value is almost as low as that of HRL-2N40 and its viscosity is considerably lower.

There is an interesting correlation between the VGM effect and the average

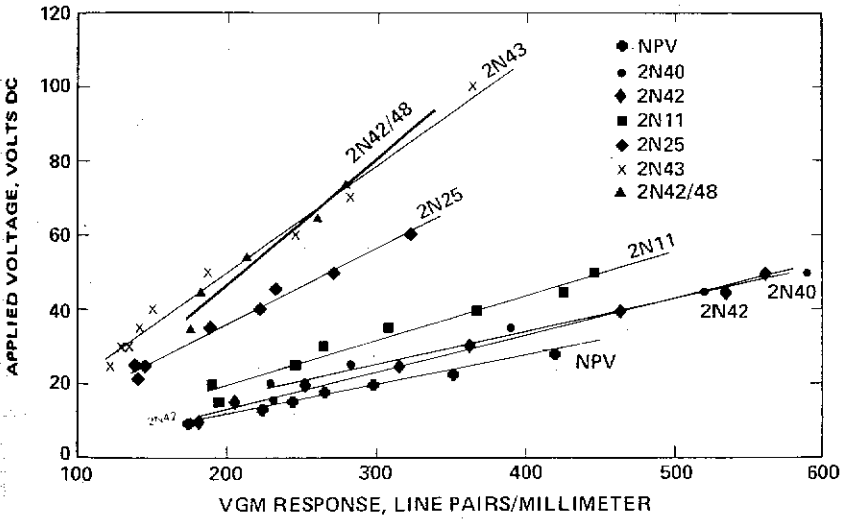

FIGURE 3 VGM voltage dependence for various liquid crystals.

molecular length of the mixtures in the RO-R′ ester series in Tables I and II. As their length increases (due to longer alkyl end groups), the V_{th} values of the first three mixtures (2N42, 2N43, and 2N42 48) increase. The longer length mixtures (2N44, 2N46 and 2N48) do not show VGM effects. Since the dielectric anisotropy ($\Delta\epsilon$) is reported[6] to have a large effect on VGM, it may be the change of $\Delta\epsilon$ with average length that causes these results. In this series the V_{th} increases as $\Delta\epsilon$ becomes more negative (with increasing length), and no VGM is observed when $\Delta\epsilon$ is -0.3 and more negative. This is similar to the VGM effects reported by Barnik *et al.*[6] for a much wider range of $\Delta\epsilon$. In a more complex series of phenyl benzoate mixtures (containing four different classes of end groups) they found that V_{th} increased as $\Delta\epsilon$ became more negative, and they also reported a critical value of $\Delta\epsilon = -0.3$. However, the critical value of $\Delta\epsilon$ apparently varies with composition of the end group classes used since our 2N25 mixture of RO-R′ and RO-OR′ esters shows VGM and has $\Delta\epsilon = -0.38$. Our latter group of three mixtures (2N11, 2N40 and 2N25), also shows a general trend of increased V_{th} with more negative $\Delta\epsilon$. The effect of $\Delta\epsilon$ appears to be less significant in these mixtures than in the RO-R′ series, but it should be noted that the 2N11 mixture is quite different in composition from the other two mixtures.

The grating lines in the VGM lie parallel to the surface alignment of the liquid crystal director in the off state. Although rubbing has proven to be satisfactory for test cells, a much more uniform homogeneous alignment can be obtained by ion-beam etching certain types of surfaces.[25] Figure 4 shows the best quality of domains that we have thus far obtained.

With the application of alternating fields of about 10 Hz, some cells were conductive enough to exhibit Williams-type domains.[26] These domains are perpendicular to the quiescent state alignment and their periodicity is only slightly affected by the applied field. The Williams domains exist in a narrow range above the threshold voltage due to dynamic scattering resulting from increasing turbulent flow within the cell as the voltage is increased.[27] This effect in conjunction with the very small variation in the spacing of domains, limits the utility of this mode as a diffraction device. For frequencies below 10 Hz, a mixed-mode behavior is observed in the more conductive cells, with VGM and Williams-type domains appearing sequentially. The cells also exhibit severe scattering during the appearance of the Williams domains, especially as the frequency is raised. We have not been able to produce pure VGM behavior with alternating fields of zero average value even for cases of very asymmetric waveforms.

The diffraction efficiency of the VGM cells depends strongly on the applied voltage, and can be as large as 25% in the second order (utilizing HRL 2N40 in a 6 μm thick cell). Interesting polarization effects of the odd and even diffraction orders as a function of the input light polarization are being investigated.

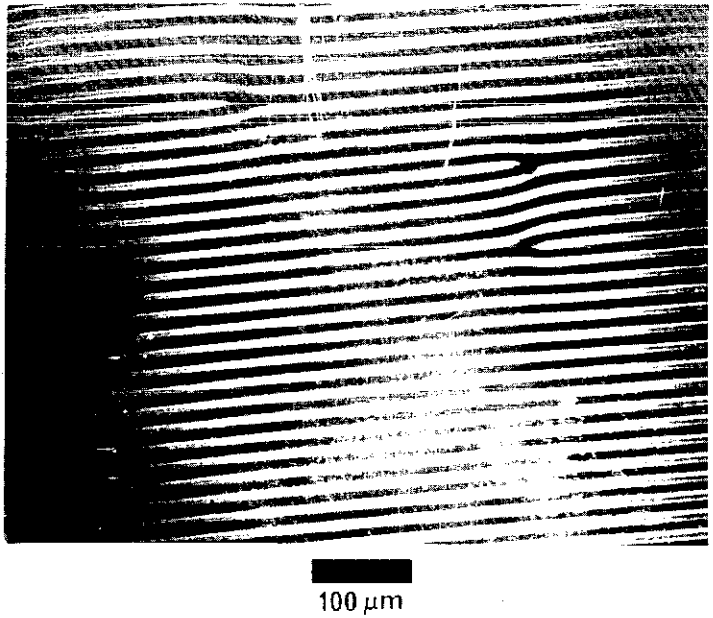

FIGURE 4 The phase grating structure of the VGM device at a fixed voltage viewed through a phase contrast microscope.

III VGM DEVICE DESCRIPTION

The structure of the present photoactivated VGM device is shown schematically in Figure 5. This configuration is similar to the dc photoactivated liquid crystal devices described previously.[28,29] The cell includes a vapor-deposited ZnS photoconductor and liquid-crystal layer placed between ITO transparent electrodes that have been deposited on glass substrates. In operation, the applied dc voltage is impressed across the electrodes.

The operating principle of the device is straightforward. The photoconductor is designed to accept most of the drive voltage when not illuminated; the portion of the voltage that drops across the liquid crystal layer is below the activation threshold of the liquid crystal VGM effect. Illumination incident upon a given area of the photoconductive layer reduces its resistance, thereby increasing the voltage drop across the liquid crystal layer and driving the liquid crystal into its activated state. Thus, because of the VGM effect, the photoconductor converts an input intensity distribution into a local variation of the phase-grating spatial frequency. The high lateral resistance of the thin photoconductive film prevents significant spreading of the photoconductivity and the associated liquid crystal electrooptic effect. As a result, the light-activation process exhibits high resolution, as will be discussed in more detail below.

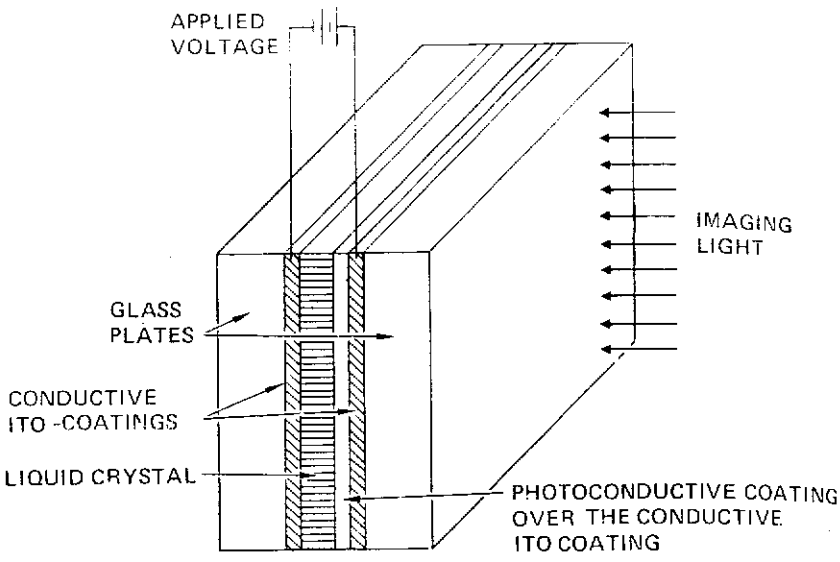

FIGURE 5 Schematic diagram of the VGM device construction. Current devices are read out in transmission at a wavelength at which the photoconductor is insensitive.

Because the VGM phenomenon is a dc instability effect occurring in high-resistivity ($\rho > 10^{10}\ \Omega - \text{cm}$) pure liquid crystal compounds, the device requires a high resistance photoconductive layer. Zinc sulfide has been selected as the photoconductor material for the best resistance match with the liquid crystal layer. Because the liquid crystal molecules are sensitive to photodecomposition in the ultraviolet, the ZnS layer is preferably made thick enough to optimize photoactivation in the blue region of the spectrum.

The ZnS layer is deposited on transparent ITO electrodes by evaporation or ion-beam-sputtering methods. The sputtered films were 0.5 μm thick, highly transparent smooth surface layers. With the evaporation technique, we produced photoconductors of 1.5 to 5 μm thickness, characterized by a hazy, rough surface appearance that caused difficulties in liquid crystal alignment parallel to the electrodes. It has been reported that vaporized ZnS causes homeotropic or tilted homeotropic orientation of the liquid crystal material.[30] Mechanical polishing of the evaporated photoconductors increased their transparency and surface uniformity, while polymer (PVA) coating the top of these ZnS layers, supplemented by additional surface treatment, resulted in good parallel alignment. Photoconductors were evaluated and compared by measuring the dark current and switching ratios of the resulting VGM devices.

From the preliminary photosensitive devices fabricated using a ZnS photoconductive layer to achieve the necessary high resistance, one cell was selected that aligned well and did not suffer the usual rapid deterioration seen in dc

operation. This deterioration is assumed to result from poisoning of the liquid crystal by the diffusion of ions from the photoconductor. This particular cell was constructed of a 5 μm thick evaporated ZnS layer that had been polished and then rubbed with surfactant polyvinyl alcohol. The counterelectrode was an ITO transparent layer treated with the same surfactant. The 6 μm thick liquid crystal layer was made of HRL-2N40 ester. The dark series resistance of the 2.5 cm square cell was measured to be 3×10^8 Ω. With -160 V applied to the photoconductor electrode and with saturation illumination of 7.3 mW/cm^2 in the passband 410 to 550 nm, the spatial frequency of the VGM domains was calculated from the observed angles of diffracted orders to be 588 lines/mm. The device threshold at this illumination was 21 V, corresponding to a grating frequency of 103 lines/mm. The optical threshold at 160 V is of the order of 50 μW/cm^2.

Planar VGM test cells were studied with respect to edge effects on resolution and possible "spillover" of domains into adjacent unactivated areas. Electrodes were specially prepared by removing sections of the conductive coating by etching. A parallel plate cell was constructed such that there were conductive areas facing each other, either with conductive edges aligned or with a maximum overlap of 150 μm of a conductive electrode over the nonconducting area. Cell spacing was 6.3 μm and the material was Merck NP-V. For alignment parallel to the edge when operating close to the threshold voltage, domains were parallel to the edge and within the active area. For higher voltages, there was fringe spillover by not more than one fringe spacing. For alignment perpendicular to the edge, domains appear to either terminate at the edge or to join with an adjacent domain. The quality of the edge behavior is shown in Figure 6. These studies indicated that implementation of the VGM effect in an image processing device should ultimately produce a resolution not limited by degradation due to edge effects.

IV NONLINEAR OPTICAL PROCESSING USING VGM DEVICES

IV.A. Implementation of point nonlinear functions

The VGM liquid crystal device can be considered to be an intensity-to-spatial frequency converter capable of operating on two-dimensional images. The intensity-to-spatial frequency conversion allows the implementation of arbitrary point nonlinearities with simple Fourier plane filters. When an input image illuminates the photoconductor surface of this device the intensity variations of the input image change the local grating frequency. If coherent light is utilized to Fourier transform the processed image, different spatial frequency components of the encoded image, corresponding to different input intensities, appear at different locations in the Fourier plane as shown in Figure 7. Within the dynamic range of the device, intensities can thus be mapped

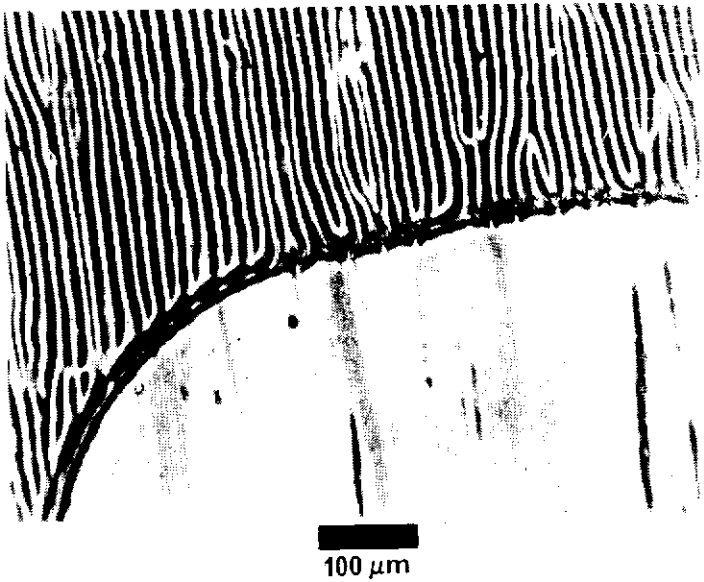

FIGURE 6 Behavior of domains near an edge.

monotonically into positions along a line in Fourier space. The input intensity distribution has thus been coded into Fourier (spatial frequency) space. If the spatial frequencies of the VGM domains are much larger than the largest spatial frequency component encountered in the images to be processed, we are in the tractable situation, familiar in communications theory, where the carrier frequency is much higher than the modulation frequencies. Thus, by placing appropriate spatial filters in the Fourier plane it is possible to obtain different transformations of the input intensity in the output plane as depicted in Figure 7b. This figure describes the variable grating mode nonlinear processing algorithm graphically. The input intensity variation is converted to a spatial frequency variation by the characteristic function of the VGM device (upper right-hand quadrant). These variations are Fourier transformed by the optical system and the spectrum is modified by a filter in the Fourier plane (upper left-hand quadrant). Finally, a square-law detection produces the intensity observed in the output plane (lower left-hand quadrant). Considered together, these transformations yield the overall nonlinearity (lower right-hand quadrant). Design of a proper spatial filter for a desired transformation is a relatively easy task. For example, a level slice transformation requires only a simple slit that passes a certain frequency band or bands. A mathematical formulation of nonlinear processing utilizing the VGM device is presented elsewhere.[31] The principal result of this analysis is the relation

$$b\nu_0 \geq 2N \tag{2}$$

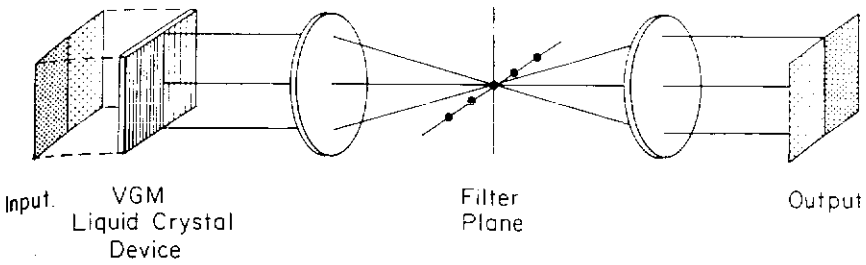

(a)

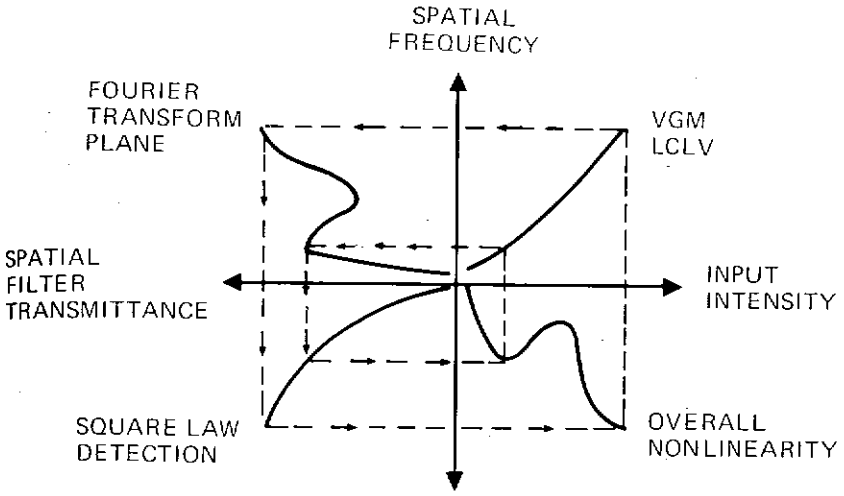

(b)

FIGURE 7 VGM nonlinear processing. (a) Experimental setup indicating the mapping of intensity to spatial frequency. (b) The overall input-output characteristic can be found by stepping through the successive nonlinear transformations including (1) the intensity to spatial frequency conversion, (2) spatial filtering, and (3) intensity detection.

where b is the pixel width, v_0 is the lowest usable VGM spatial frequency, and N is the number of distinguishable grey levels. This relation requires that the pixel size contains $2N$ periods of the lowest grating frequency if N grey levels are to be processed. For example, a 100×100 pixel image could be processed with 50 distinguishable grey levels on a 50 mm square device with $v_0 = 200$ cycles/mm.

The ability to perform arbitrary point nonlinearities over two-dimensional images greatly increases the flexibility of optical processing system. In the past few years several different approaches to the problem of implementing gener-

alized nonlinearities have been investigated. These have included halftone screen techniques,[7,8] nonlinear devices,[9,10] feedback methods,[11] and variable level slice[12] among others. The main advantage of the VGM approach over previous methods is the ease of programming the functional nonlinearity desired for a given image transformation. This is done simply by changing the transmittance distribution of the spatial filter in the optical processing system. The spatial filter is of relatively low resolution and need only have a space-bandwidth product equal to the number of gray levels to be processed independent of the space-bandwidth product of the input image.

The same programmability advantage applies to the implementation of binary logic operations. One device can be used to implement any of the combinatorial logic operations (AND, OR, XOR, and their complements) by simply changing a Fourier plane filter. Previously described optical logic systems were "hardwired" to perform specific operations.[13-20] In most cases one or more logic functions proved difficult or cumbersome to implement. Use of the VGM liquid crystal device for the implementation of combinatorial logic operations is described below.

IV.B. Demonstration of a level slice function with the VGM device

In this experiment the ability of the VGM device to generate a level-slice nonlinearity is demonstrated. The experimental arrangement is shown in Figure 8. A continuous tone input picture is illuminated by an arc lamp source and imaged onto the photoconductor surface of a VGM device which initially exhibits a uniform phase grating structure due to a dc bias voltage. The grating period is locally modulated by the input picture intensity, and this modulation is mapped into a position along a line in the spatial filter plane. A red filter ensures that only the readout laser beam enters the coherent optical processor.

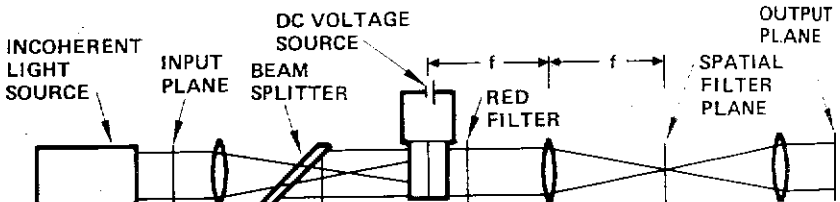

FIGURE 8 Experimental setup used to perform the level slice experiments. The spatial filter was a variable annular aperture.

Sectors of small circular annuli of varying radii are used to pass certain spatial frequency bands. This in effect allows only prescribed input intensity ranges to appear in the output. Circular rather than straight slits are used to capture the weak light which in small part is diffracted into circular arcs (see Figure 2) because of the grating imperfections (see Figure 1). Figure 9 shows both the input and level sliced output pictures. Figure 9a shows a positive print of the original image as photographed on the imaging screen. A negative of the original was used in the experiments. Figure 9b shows a low intensity level slice corresponding to a VGM spatial frequency of 120 lines/mm with approximately 3% bandwidth. In Figure 9c another level, corresponding to 153 lines/mm, is shown. Figure 9d at 236 lines/mm illustrates the interference from second harmonics. Weak second harmonics of the low intensity image slice corresponding to 118 lines/mm can appar in the 236 lines/mm level slice. In Figure 9e, a broader slice of approximately 11% bandwidth was taken centered about the level corresponding to 140 lines/mm. This picture may be compared with the previous slices and particularly with the slice shown in Figure 9c. Finally, Figure 9f shows a very high input intensity slice at 440 lines/mm with 10% bandwidth. Three grey levels may be seen simultaneously, these correspond to the superposition of three broad intensity slices.

IV.C. VGM implementation of logic functions

To see how the VGM device can be used to implement binary logic operations, one need only realize that the function of a logic circuit can be represented as a simple binary nonlinearity operating on the incoherent superposition of two

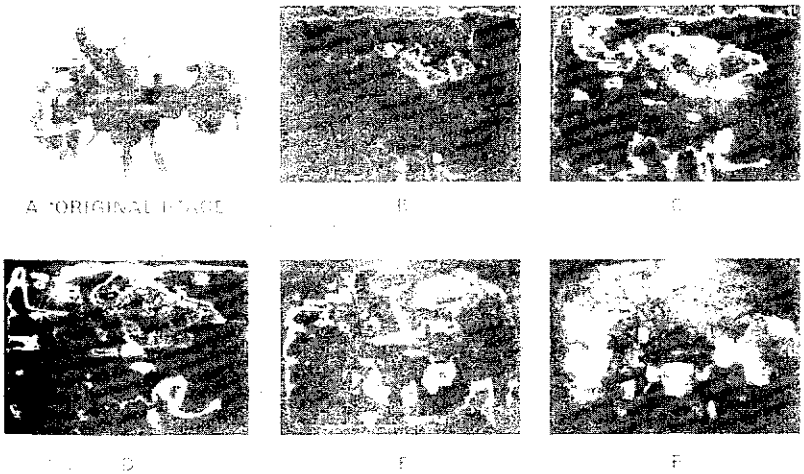

FIGURE 9 Level slice results. (a) Original image *b-f*) Level slice results for various apertures as discussed in the text.

binary images as input. As shown in Figure 10, NOT is simply a hard-clipping inverter, while AND and OR are hardclippers with different threshold and XOR is a level slice function.

The VGM device is well suited to implementing this type of nonlinearity. Since the nonlinearities associated with logic operations are binary functions, they can be implemented with simple slit apertures, i.e., 0 or 1 transmittance values. A noteworthy advantage of the VGM approach over previous optical logic methods[17–20] is the ease of programming the nonlinearity, by merely changing the aperture in the spatial frequency plane.

Another feature of the VGM technique that is especially suitable for logic processing is that the input and output are physically separate beams. The input beam modulates a photoconductor; concurrently the image is read out with a second beam. This separation of input and output provides for the possibility of restoring the output levels to the desired 0 and 1 values even if the input levels are not exactly correct. This feature is essential to the production of a reliable logic system that is immune to noise and systematic errors in the levels. Electronic logic elements possess such level restoring capability, but currently proposed optical logic schemes[17–20] lack this essential characteristic.

A series of experiments were conducted to demonstrate the fundamental logic functions. Two input fields were superimposed at the VGM plane along with a bias illumination. The total illumination intensity on the photoconductor of the VGM device was thus the sum of the two input intensities and the bias intensity. The input illumination was filtered high-pressure mercury arc lamp. The bias illumination was provided by a collimated tungsten bulb source. The VGM device was read out in transmission using a HeNe laser. A

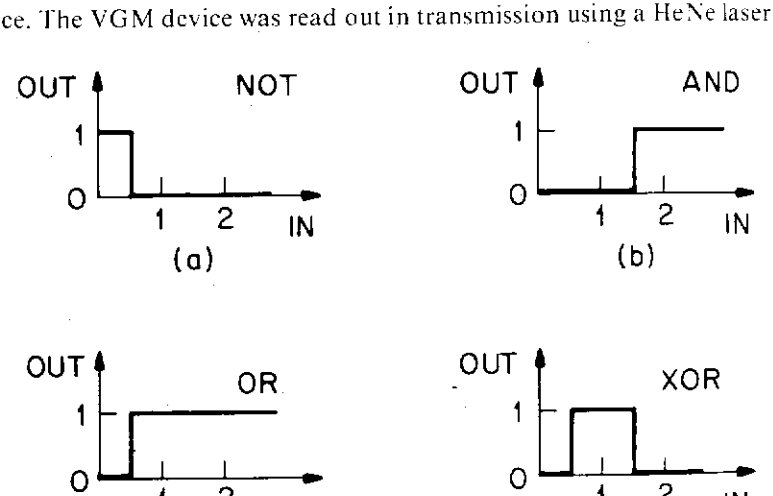

FIGURE 10 Logic functions as simple nonlinearities. Given an input consisting of the sum of two binary inputs, different logical operations can be effected on those inputs by means of the depicted nonlinear characteristics. (a) NOT, (b) AND, (c) OR, (d) XOR.

filter was placed in the Fourier plane to select the desired spatial frequencies for each logic function.

For these experiments, the inputs consisted of one vertical rectangular aperture and one horizontal aperture. When these were superimposed along with the bias, a square image was formed with the four quadrants having the intensity levels shown in Figure 11. This image corresponds to the logic truth table

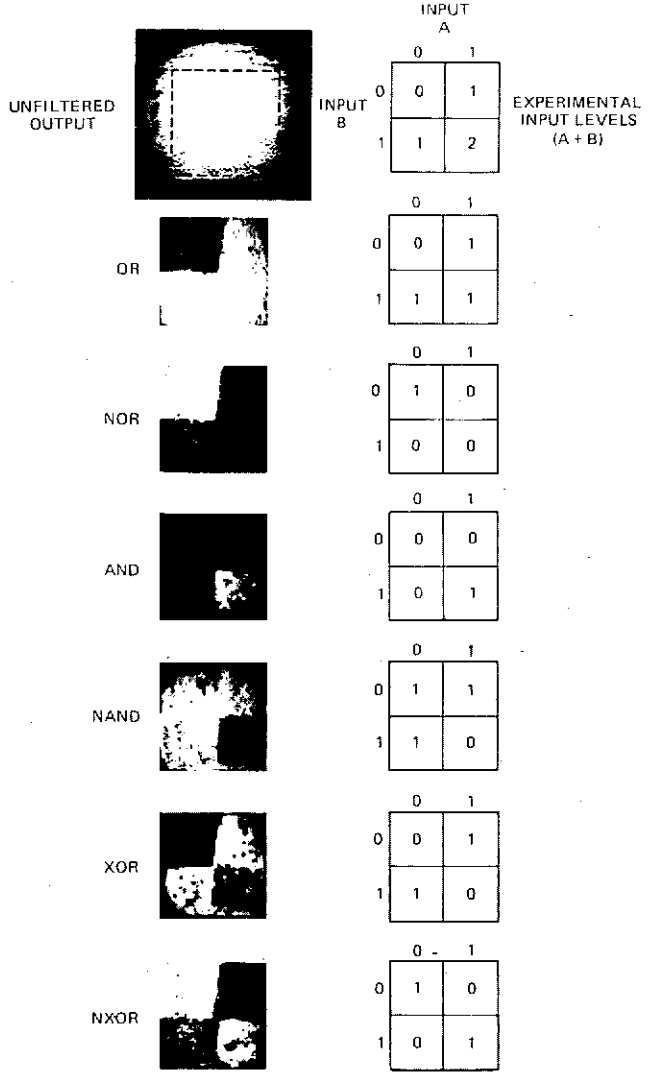

FIGURE 11 VGM logic results. The right-hand column indicates ideal output levels for an image consisting of four quadrants corresponding to truth table values. The left-hand column shows the corresponding experimental results. The first row shows the input for all experiments which consisted of a superposition of two binary images. Succeeding rows show results for the logic operations OR, NOR, AND, NAND, XOR, and NXOR, respectively.

shown. Thus the output images have intensity levels determined by the truth table associated with the desired logic function. The logic functions AND, OR, XOR and their complements were implemented sequentially as shown in Figure 11 by altering only the Fourier plane filter. Imperfections visible to the output plane data arise from defects in the cell structure of the VGM device employed in these experiments.

A more complete discussion of VGM logic implementation can be found in Ref. (32).

V CONCLUSION

The variable grating mode effect can be incorporated in a photoconductively-addressed device structure which provides an overall intensity-to-spatial frequency conversion. The optical processing experiments using the VGM liquid crystal device described in this paper demonstrate the potential of this real time optical image transducer for numerous parallel nonlinear operations on images. The molecular origin of the VGM phenomenon is now being studied in connection with the behavior of the VGM phase grating as observed by polarization microscopy and polarization-dependent optical diffraction. Improvements in such characteristics of the device as response time, uniformity, dynamic range and density of defects are under continuing investigation.

Acknowledgments

We gratefully acknowledge the helpful contribution of M. Piliavin in the early phase of this work. This project was sponsored by the Air Force Office of Scientific Research under Grant AFOSR-77-3285 at USC and Contract F49620-77-C-0080 at HRL. Liquid crystal work on the project was partially supported by the Air Force Office of Scientific Research on Contract F49620-77-C-0017 at HRL.

References

1. L. K. Vistin'. *Sov. Phys. Dokl.*, **15**, 908 (1971).
2. W. Greubel and W. Wolf, *Appl. Phys. Lett.*, **19**, 213 (1971).
3. J. M. Pollack and J. B. Flannery, in *Liquid Crystals and Ordered Fluids* J. F. Johnson and R. E. Porter, eds. (Plenum Press, New York, 1978), **2**, 557.
4. J. M. Pollack and J. B. Flannery, *Society for Information Display 1976 Intern. Symp. Digest*, 143 (1976).
5. P. K. Watson, J. M. Pollack and J. B. Flannery, in *Liquid Crystals and Ordered Fluids*, J. F. Johnson and R. E. Porter, eds. (Plenum Press, New York, 1978), **3**, 421
6. M. I. Barnik, L. M. Blinov, A. N. Trufanov and B. A. Umanski, *J. de Physique*, **39**, 26 (1978).
7. H. Kato and J. W. Goodman, *Appl. Opt.*, **14**, 1813 (1975).
8. T. C. Strand, *Opt. Commun.*, **15**, 60 (1975).
9. S. R. Dashiell and A. A. Sawchuk, *Appl. Opt.*, **16**, 1009 (1977).
10. S. R. Dashiell and A. A. Sawchuk, *Appl. Opt.*, **16**, 2279 and 2394 (1977).
11. B. J. Bartholomew and S. H. Lee, *Appl. Opt.*, **19**, 201 (1980).

12. A. Tai, F. Cheng and F. J. S. Yu, *Appl. Opt.*, **16**, 2559 (1977).
13. D. Casasent, *Opt. Eng.*, **19**, 228 (1974).
14. S. Iwasa and J. Feinleib, *Opt. Eng.*, **13**, 235 (1974).
15. A. Armand, A. A. Sawchuk, T. C. Strand, D. Boswell and B. H. Soffer, *Opt. Lett.*, **5**, 129 (1980).
16. J. D. Michaelson and A. A. Sawchuk, *Proc. Soc. Photo Opt. Instrum. Engin.*, **218**, 107 (1980).
17. R. A. Athale and S. H. Lee, *Opt. Eng.*, **18**, 513 (1979).
18. S. A. Collins, Jr., U. H. Gerlach and Z. M. Zakman, *Proc. Soc. Phot. Opt. Instrum. Eng.*, **185**, 36 (1979).
19. D. H. Schaefer and J. P. Strong, III, *Proc. IEEE*, **65**, 129 (1977).
20. L. Goldberg and S. H. Lee, *Appl. Opt.*, **18**, 2045 (1979).
21. J. B. Margerum, J. E. Jensen and A. M. Lackner, *Mol. Cryst. Liq. Cryst.* (in press).
22. A. D. Jacobson, *Development of a Reflective Mode Liquid Crystal Light Valve*, NAVSEA Contract N0024 73 C 1185 Final Report (May, 1975).
23. H. S. Lim and M. J. Little, USP 4,128,312 (Dec. 5, 1978).
24. J. D. Margerum, *Anisotropic and Electro-Optical Effects in Liquid Crystals*, AFOSR Contract N49620-77-C-0017 Final Report, (March 1981).
25. M. J. Little, H. L. Garvin and L. J. Miller, in *Liquid Crystals and Ordered Fluids*, J. F. Johnson and R. E. Porter, eds. (Plenum Press, New York, 1978) **3**, 497.
26. R. Williams, *J. Chem. Phys.*, **39**, 384 (1963).
27. G. H. Heilmeier, L. A. Zanoni and L. A. Barton, *Proc. IEEE*, **56**, 1162-(1968).
28. J. D. Margerum, J. Nimoy and S. Y. Wong, *Appl. Phys. Lett.*, **17**, 51 (1970).
29. J. D. Margerum, T. D. Beard, W. P. Bleha and S. Y. Wong, *Appl. Phys. Lett.*, **19**, 216 (1971).
30. H. Kruger, H. F. Mahlim and W. Rauscher, U.S. Pat. 4, 112, 157, September 1978.
31. B. H. Soffer, D. Boswell, A. M. Lackner, P. Chavel, A. A. Sawchuk, T. C. Strand and A. R. Tanguay, Jr., *Proc. Soc. Photo-Opt. Instrum. Eng.*, **232**, 128 (1980).
32. P. Chavel, A. A. Sawchuk, T. C. Strand, A. R. Tanguay, Jr. and B. H. Soffer, *Opt. Lett.*, **5**, 398 (1980).